Nano Research

ISSN 1998-0124 CN 11-5974/O4
https://doi.org/10.1007/s12274-024-6970-1

Research Article

Exploring the potential of simple automation concepts for quantifying functional groups on nanomaterials with optical assays

Isabella Tavernaro (✉), Anna Matiushkina, Kai Simon Rother, Celina Mating, and Ute Resch-Genger (✉)

Federal Institute for Materials Research and Testing (BAM), Division Biophotonics, Richard-Willstaetter-Str. 11, Berlin 12489, Germany

Received: 19 June 2024 / **Revised:** 4 August 2024 / **Accepted:** 15 August 2024

ABSTRACT

Until now, automation in nanomaterial research has been largely focused on the automated synthesis of engineered nanoparticles (NPs) including the screening of synthesis parameters and the automation of characterization methods such as electron microscopy. Despite the rapidly increasing number of NP samples analyzed due to increasing requirements on NP quality control, increasing safety concerns, and regulatory requirements, automation has not yet been introduced into workflows of analytical methods utilized for screening, monitoring, and quantifying functional groups (FGs) on NPs. To address this gap, we studied the potential of simple automation tools for the quantification of amino surface groups on different types of aminated NPs, varying in size, chemical composition, and optical properties, with the exemplarily chosen sensitive optical fluorescamine (Fluram) assay. This broadly applied, but reportedly error-prone assay, which utilizes a chromogenic reporter, involves multiple pipetting and dilution steps and photometric or fluorometric detection. In this study, we compared the influence of automated and manual pipetting on the results of this assay, which was automatically read out with a microplate reader. Special emphasis was dedicated to parameters like accuracy, consistency, achievable uncertainties, and speed of analysis and to possible interferences from the NPs. Our results highlight the advantages of automated surface FG quantification and the huge potential of automation for nanotechnology. In the future, this will facilitate process and quality control of NP fabrication, surface modification, and stability monitoring and help to produce large data sets for nanomaterial grouping approaches for sustainable and safe-by-design, performance, and risk assessment studies.

KEYWORDS

automation, quantification of amino groups, fluorescamine assay, amorphous silica nanoparticles, iron oxide nanoparticles, upconversion nanoparticles

1 Introduction

Laboratory automation, which was initiated in the early 1990s in the fields of biomarker research, drug discovery, and clinical assays to reduce analysis time and costs, increase sample throughput, and advance miniaturization to reduce sample size or amount [1–9], has meanwhile reached bio-, environmental, and food analysis [1, 2, 10], as well as material chemistry [11, 12] and nanotechnology. Examples for the latter present the automated syntheses of engineered nanoparticles (NPs) including the screening of synthesis parameters to speed up the identification of NP morphologies and chemical compositions providing optimum functionality, to improve the reproducibility of NP fabrication or to simplify frequent steps of NP preparation such as purification [13–22]. For functional optical NPs like semiconductor quantum dots, perovskites, lanthanide-based upconversion nanoparticles (UCNPs), and plasmonic metal NPs, these approaches often involve in-line or at-line optical detection methods. Examples for increasingly automated NP characterization methods present imaging methods like electron microscopy [23, 24]. Also, first examples for toxicity testing of nanomaterials utilizing automated optical microscopy platforms have been reported which require the analysis of many samples [25].

Although the importance of NP surface chemistry is well known for application-relevant properties such as dispersibility and colloidal stability as well as NP function, only recently, its huge impact on the interaction of NPs with the environment and biological species was recognized, determining NP cellular uptake, and hazard potentials [26–29]. The increasing need to improve the quality control of NP fabrication and surface modification processes, and for stability monitoring—together with safety concerns of the EU commission, international standardization organizations, and regulators—call for simple, robust, inexpensive, and reliable methods for determining and screening NP surface chemistry [29, 30]. However, until now, automation schemes have not yet been utilized for methods providing information on NP surface chemistry. Amongst the many different analytical methods utilized for quantifying functional groups (FGs) on NPs, optical methods such as photometry and fluorometry are particularly promising as they offer a high sensitivity, specificity, and speed of analysis at relatively low costs [31]. Optical assays have been developed for surface FGs like amino, carboxyl, aldehyde, maleimide, and thiol groups as well as for NP-bound biomolecules like proteins [32]. Typical examples are the Ninhydrin, N-succinimidyl-3-(2-pyridyldithio) propionate (SPDP), fluorenylmethoxycarbonyl- (Fmoc), and fluorescamine (Fluram) assays [30]. While the performance of optical assays is straightforward, however, the workflows can involve multiple

Address correspondence to Isabella Tavernaro, isabella.tavernaro@bam.de; Ute Resch-Genger, ute.resch@bam.de

steps, such as dilution, transfer of defined volumes of liquids, and incubation and washing steps that can be time consuming and error prone. Moreover, the optical properties of reporter dyes such as fluorescence, can be affected by pH and matrix. This can limit the data consistency even for skilled and trained staff.

This encouraged us to explore the potential of automation tools successfully applied in other research fields for the quantification of surface amino groups on aminated silica NPs, iron oxide NPs (IONPs), and UCNPs, chosen based upon their different optical properties and their frequent usage in the life sciences [33–36], with the exemplarily chosen Fluram assay. This fast, selective, and sensitive assay is broadly applied for the quantification of primary amino (NH_2) groups on pharmaceutical compounds, biomolecules, and surface-modified nano- and microparticles like polymer and silica particles [37–40]. It exploits the quantitative reaction of the precursor fluorophore fluorescamine (4'-phenyl-3H,3'H-spiro [2-benzofuran-1,2'-furan]-3,3'-dione) with primary amino groups, yielding a colored and fluorescent product [37–39]. The reaction conditions of the Fluram assay as well as the emission intensity and stability of the fluorescent product are, however, influenced by pH and solvent [41]. In addition, this assay involves several pipetting and dilution steps, which are mainly performed manually in research labs and small enterprises in the field of nanotechnology. The uncertainty of these steps largely depends on the proper function of the commonly employed air-cushion pipettes, which must be regularly calibrated, as well as on operator skills and sample properties like viscosity [42–44]. Hence, a reliable and accurate quantification of NH_2 groups with the Fluram assay requires target-specifically optimized, precisely controlled, and preferably standardized conditions. In addition, for NPs, also NP-inherent optical properties such as absorption and emission as well as size-dependent scattering could affect assay performance and results. This is addressed in our study by comparing the quantification of NH_2 groups on aminated silica NPs, IONPs, and UCNPs, with manually performed and automated Fluram assays and automated readout with a microplate reader in fluorescence mode using positive and negative control samples to account for the optical properties of the different aminated NPs. Overall, our results clearly demonstrate the advantages of an automated FG characterization with respect to data reliability, consistency, and speed of analysis and highlight the underexplored potential of automation for such simple optical tools for the screening, monitoring, and quantification of surface FGs on nanomaterials. Our study is expected to pave the road for adapting automation concepts developed for bioanalytical assays with optical detection to applications in nanotechnology in the future.

2 Experimental

2.1 Materials

All chemicals, reagents, and solvents were of analytical grade or higher and used as received, unless otherwise stated. All aqueous solutions and buffers were prepared with MilliQ-water (0.055 µS/m; Merck Milli-Q® IQ 700 device).

2.2 Nanoparticle syntheses and characterization

Pristine silica NPs (SiO_2 NP) [45], iron oxide/silica core/shell NPs (SiO_2@IONP) and upconversion/silica core/shell NPs (SiO_2@UCNP) [46] were synthesized following literature protocols. Surface amino FGs were introduced by a postsynthetic grafting step with (3-aminopropyl)triethoxysilane (APTES) as detailed in the Electronic Supplementary Material (ESM). NP properties like size, shape, and surface charge were characterized by transmission electron microscopy (TEM), dynamic light scattering (DLS), and zeta potential measurements using a Talos F200S Microscope (ThermoFisher Scientific) and a Malvern Panalytical Zetasizer Nano ZS equipped with a 630 nm laser. The zeta potential was calculated from the NP electrophoretic mobility using the Einstein-Smoluchowski theory.

2.3 Quantification of the total and derivatizable number of amino FGs

The total amount of amino FGs was potentiometrically determined by a back titration of the aminated NPs, dispersed in 0.1 mM hydrochloric acid (ChemSolute GmbH), with 0.1 mM sodium hydroxide solution (ChemSolute GmbH) using a SevenExcellence S475 pH meter from Mettler Toledo (Germany) and the derivatizable number of amino FGs by the fluorescamine (Fluram) assay. This assay was manually performed by 11 operators and additionally done with the Assist Plus automated pipetting system (INTEGRA Biosciences, Switzerland), equipped with a D-One 1250 µL 1-channel pipette and a D-One 300 µL 1-channel pipette with the specific TipGrips (INTEGRA Biosciences) and the software VIALAB (version 3.1.0). For manual pipetting, different sets of Eppendorf Research Plus pipettes (single-channel, variable) including volume ranges 0.5–10 µL (medium grey), 2–20 µL (light grey), 2–20 µL (yellow), 10–100 µL (yellow), 20–200 µL (yellow), 30–300 µL (orange), and 100–1000 µL (blue) with the recommended epT.I.P.S. (Eppendorf) were employed, all calibrated, see ESM for more details. For the Fluram assay, fluorescamine (1.51 µmol, 15 µL, abcr GmbH, Germany), dissolved in acetonitrile (Sigma Aldrich, Germany) was added to the previous purified NP samples (0.2–0.5 mg), ethanolamine (EA) samples (Sigma Aldrich, Germany; 12 different concentrations) used for the calibration curve, and the negative (pristine NPs) and positive (l-valine) controls, all in 1 mL of phosphate buffer (0.01 M, pH 8), assay readout was done with the Infinite M200 pro microplate reader from Tecan (Switzerland) using an excitation wavelength λ_{ex} of 392 nm and an emission wavelength λ_{em} of 480 nm. The detailed NP characterization, FG quantification, including protocols and calculations of the potentiometric back titration, optical assays, and calculations of NP surface area (m^2/g), number of NP per mg, and number of amino FGs per particle are provided in the ESM.

3 Results and discussion

3.1 Nanoparticle synthesis and characterization

The four types of aminated NPs, representatively selected for manual and automated surface FG quantification with the Fluram assay, are shown in Fig. 1. This included one commercial NP (NanoChOp-01) with a nominal diameter of around 50 nm and a polydispersity index of 0.10 [47], and three custom-made spherical, aminated core and core/shell NPs with sizes < 25 nm, i.e., an aminated amorphous silica NP (SiO_2 NP-NH_2) as well as an IONP and a lanthanide-based UCNP ($NaY_{0.5}Gd_{0.3}F_4$:Yb, Er). The latter two NPs were coated with amorphous silica shells bearing amino FGs (SiO_2-NH_2@IONP; SiO_2-NH_2@UCNP). These NPs, which are broadly utilized in the life sciences [33–36], were chosen because of their different optical, i.e., scattering, absorption, and fluorescence features, to examine a possible influence of these NP properties on the assay results (see Figs. S5(a) and S5(b) in the ESM).

Surface amination with APTES (Fig. 1(b)) was confirmed by the resulting positive zeta potential values (Fig. 1(c)). SiO_2-NH_2@IONP (d_{TEM} = 22.1 ± 1.6 nm) and SiO_2-NH_2@UCNP (d_{TEM} = 17.8 ± 1.4 nm) also showed slightly increased number-based hydrodynamic diameters of 99 ± 28 and 102 ± 29 nm after APTES grafting (Fig. 1(d) and Fig. S4 in the ESM). Using the

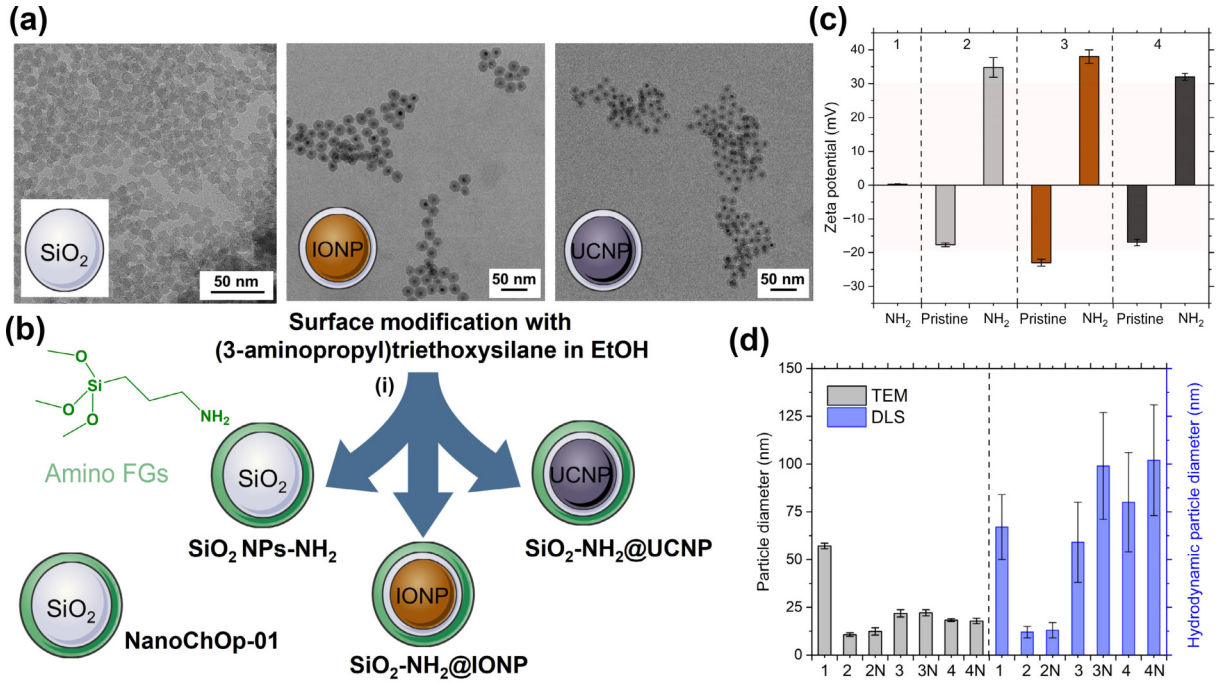

Figure 1 Overview of NP syntheses and characterization. (a) TEM micrographs of SiO_2 NP, SiO_2@IONP, and SiO_2@UCNP. (b) Surface modification with APTES (i): EtOH 30 °C, Ar, 2 days. (c) Zeta potential data measured in MilliQ-water at pH 6.6 or EtOH. (d) Diameters of (1) NanoChOp-1, (2) SiO_2 NPs, (2N) SiO_2 NPs-NH_2, (3) SiO_2@IONP, (3N) SiO_2-NH_2@IONP, (4) SiO_2@UCNP, and (4N) SiO_2-NH_2@UCNP obtained from TEM and number-based hydrodynamic diameters derived from DLS (see also Figs. S1–S4 in the ESM).

particle sizes obtained by TEM (Fig. 1, Figs. S1 and S2 in the ESM) and a silica density of 1.80 g/cm^3, an estimated monolayer of amino FGs was calculated for each particle [48], assuming 4 APTES molecules/nm^2. This yielded amino FGs amounts of 387.6 nmol/mg (NanoChOp-01), 1002.1 nmol/mg (SiO_2-NH_2@IONP), 1208.3 nmol/mg (SiO_2-NH_2@UCNP), and 1606.7 nmol/mg (SiO_2 NPs-NH_2). The total amount of amino FGs per NP was determined by potentiometric acid-base back titration and then used to calculate the surface amino FG density as a fractional monolayer coverage according to Y. Sun et al. [49]. This quantity equals the measured total number of amino FGs divided by the number of amino FGs estimated for monolayer coverage, see also ESM. As revealed in Fig. 2(a), all NPs showed a comparable amino FG coverage of about 1.5-layer, i.e., 1.49 (5.96 amino FGs/nm^2) for NanoChOp-01, 1.57 (6.60 amino FGs/nm^2) for SiO_2 NPs-NH_2, 1.38 (5.30 amino FGs/nm^2) for SiO_2-NH_2@IONP, and 1.68 (6.50 amino FGs/nm^2) for SiO_2-NH_2@UCNP.

3.2 Fluram assay

The broadly applied Fluram assay relies on the chromogenic reporter fluorescamine, which forms an optically detectable product with primary amino FGs, that absorbs between 230 and 400 nm and emits in the wavelength range of about 400–600 nm [39]. The absorption and emission features of the readout assay reaction product are distinguishable from those of fluorescamine, which absorbs at wavelength < 400 nm and is non-emissive (see Fig. S5 in the ESM). Therefore, and as the assay product remains on the NP surface, washing steps can be circumvented [30, 50, 51]. This renders this fast, selective, and sensitive assay, which has been used before in high-throughput formates, e.g., for detecting N-acyl-L-homoserine lactone (AHL) acylases and screening nanomaterial-protein interactions [50, 51], ideal for our simple automation approach for quantifying surface amino groups on aminated NPs. Moreover, this versatile concept of FG determination with optical assays and chromogenic reporters can be expanded to the determination of other common surface functionalities or NP ligands as chromogenic reporters are also known for other application relevant FGs [52–54]. Like all methods involving the labeling with a molecular reporter, the Fluram assay yields the number of derivatizable amino FGs. This number, which is relevant for the subsequent NP derivatization with, e.g., recognition moieties, biomolecules, and antifouling species [30], is affected by reporter size and shape and commonly smaller than the total number of FGs obtained with label-free methods or with very small reporters such as protons or hydroxide ions [55]. Although the number of the derivatizable FGs does not provide the exact coverage of amino groups, this number is very relevant for NP process and quality control and can be utilized as a direct measure for the reproducibility of NP synthesis and NP surface modification as well as for NP aging. Excluding interactions and steric effects, we calculated a maximum number of 1.1 reporter molecules per nm^2, for the Fluram assay and the respective chromogenic reporter. This can maximally lead to a 27.5% coverage of the estimated total number of amino FGs (Fig. 2(b)).

To explore the potential of automation for NP surface analysis, exemplarily for the four aminated NPs shown in Fig. 1, revealing different optical properties, and the Fluram assay, the pipetting steps required for assay performance and assay calibration were performed with a self-programmed pipetting robot and manually by 11 scientists and lab technicians. The automatically and manually filled microtiter plates were then read out with a microplate reader in fluorescence mode following an automated workflow. Assay readout and data analysis were done by one experienced scientist.

Prior to the automation of the Fluram assay and the comparison of automated and manual pipetting workflows, the assay parameters were optimized using the amino acid l-valine (Figs. S7 and S11 in the ESM). Thereby, we assured that for this reportedly error-prone assay, no systematic errors, originating from the pH- and solvent dependence of the reaction of fluorescamine with NH_2 groups and the pH- and time dependence of the fluorescence intensity of the optically detected assay product affected our study [41, 51]. Based upon the

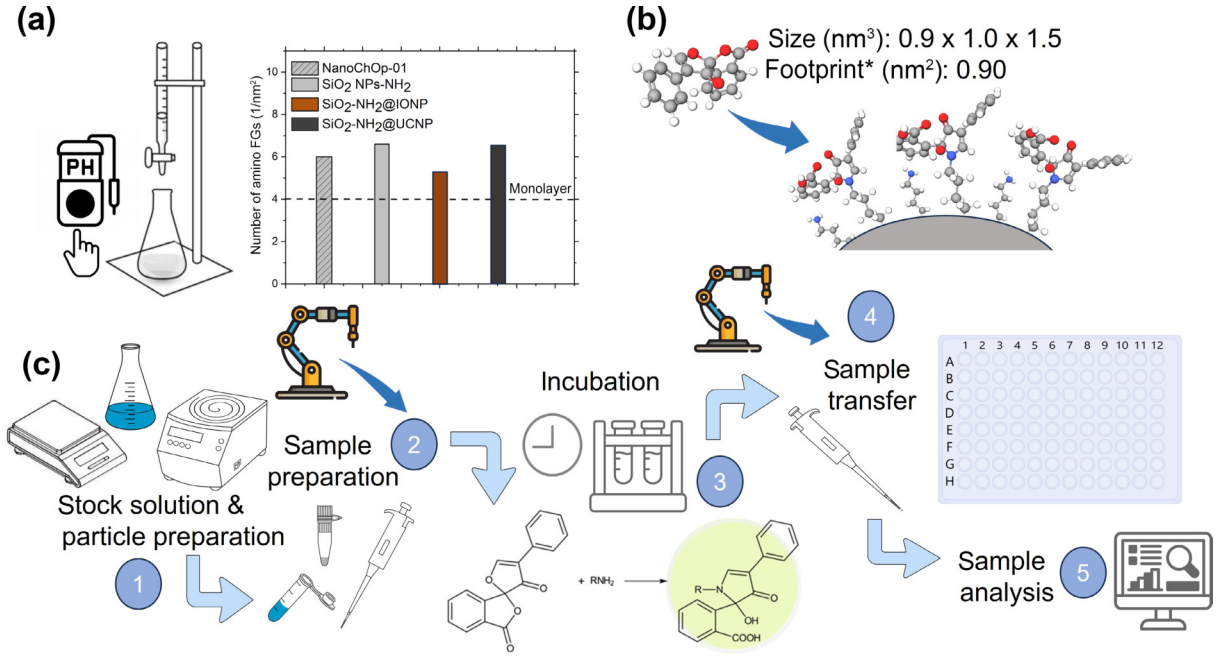

Figure 2 Overview of the methods used to quantify the total and derivatizable amount of amino FGs. (a) Manually performed acid-base back titration of the aminated NPs providing the total amount of amino FGs, here about 5.30–6.60 amino FGs per nm². (b) Scheme of the reaction of fluorescamine with surface amino FGs and estimated steric demand of the reporter on the NP surface; the footprint was estimated as the area of the smallest face of the oriented bounding box without considering steric hindrances. (c) Workflow of the 5 step Fluram assay. Automation with a pipetting robot was done for step 2 (sample preparation) and step 4 (sample transfer).

determination of the stability of the fluorescent assay product, we could guarantee a stable fluorescence signal for at least 3 h under our assay conditions (Figs. S6–S8 in the ESM). Possible influences of size- and material-dependent scattering of the targeted aminated NPs and possible interferences from NP absorption and/or fluorescence (Fig. 3(c) and Fig. S9 in the ESM) were minimized by using excitation (λ_{ex}) and emission wavelengths (λ_{em}) of 392 and 480 nm for the later assay readout. In addition, plain NPs of similar size and core composition were used as negative controls (Fig. 3(d) and Fig. S10 in the ESM).

Subsequently, the amount of surface amino FGs of the four aminated NPs shown in Fig. 1 was determined with the optimized Fluram assay. An overview of the Fluram assay workflow and the pipetting scheme including assay calibration and the chosen positive and negative controls is displayed in Fig. 2(c) and Fig S12 in the ESM. The automation of the Fluram assay with the pipetting robot was realized for step 2 (sample preparation) and step 4 (sample transfer) of the assay workflow (Fig. 2(c)). The relatively simple and cost-efficient pipetting robot used in this study by one scientist was chosen due to its self-explanatory software and ease of programming. This allowed for the straightforward customization of the pipetting parameters to suit the specific requirements of the assay by controlling volume, speed, and mixing of the sample pickup and dispensing with a motor. Details on the programming of the pipetting robot are provided in Section S6.4 in the ESM. All automatically and manually filled microtiter plates were then readout with a microplate reader in fluorescence mode, following an automated workflow drafted by an experienced scientist. This scientist was also responsible for the analysis of all assay data as mentioned before. Subsequent quantification of the surface FGs on the four aminated NPs was achieved with the aid of the assay calibration curve, recorded for the reaction of fluorescamine with different concentrations of EA.

This provided the basis for correlating the fluorescence intensities measured for the aminated particles to the amount of NH_2 groups, thereby also considering the optical signals from the negative controls.

3.3 Comparing the automated and manual performance of the Fluram assay

To determine relative standard deviations and batch-to-batch variabilities for the automated Fluram assay shown in Fig. 3, the assay was performed on three different days with two separately prepared sample sets (set1, set2). As summarized in Fig. 3(a), all assay calibration curves showed a good precision with values in the range of the systematic error of the pipettes and the particle measurements resulted in a good comparability between the two sample sets and the expected range of fluorescamine coverage on the particle surface (< 27.5% of the total amount of amino FG) with 50 ± 9 nmol/mg (set 1) and 59 ± 11 nmol/mg (set 2) for NanoChOp-01, 206 ± 33 nmol/mg (set 1) and 352 ± 42 nmol/mg (set 2) for SiO_2 NP-NH_2 and 168 ± 28 nmol/mg (set 1) and 201 ± 22 nmol/mg (set 2) for SiO_2-NH_2@UCNP, independent of potential influences of the optical properties of the NPs. With values of 698 ± 21 nmol/mg (set 1) and 653 ± 20 nmol/mg (set 2), only SiO_2-NH_2@IONP showed a higher coverage density of around 50%, even for the consideration of the optical properties of the IONPs with the aid of a correction factor derived from measurements with the unmodified SiO_2@IONP. This could point to a potential influence of the IONPs on the Fluram assay that will be systematically assessed in the future.

For the Fluram assays manually performed by 11 scientists and lab technicians with calibrated pipettes according to the previously optimized standard operation procedure (SOP), the scientific background and pipetting expertise of each participant were specified with the aid of a questionnaire (see for mor details in Section S7 in the ESM). This allowed for a more specific evaluation of the generated data. In addition, also information on sample preparation, pipetting technique, and possible errors observed by the participant during pipetting was documented. This additional information is summarized in Figs. S17–S21 and Table S2 in the ESM. Thereby, main variations in assay results could be linked to uncertainties of the pipetting steps as the systematic errors of the different calibrated pipettes employed in this study varied depending on the pipetted volume, highlighting

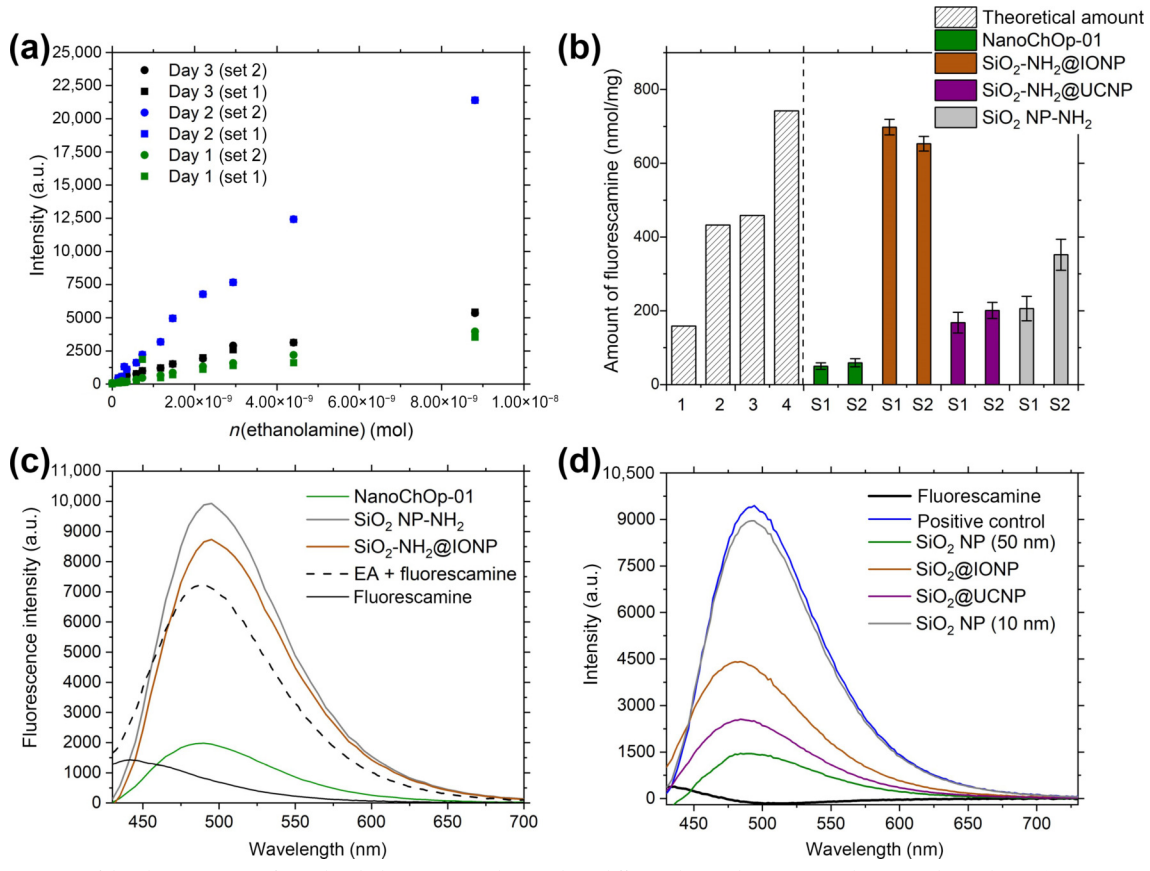

Figure 3 Overview of the Fluram assay performed with the pipetting robot on three different days with two separately prepared sample sets (set 1 (S1), set 2 (S2)) by one scientist to determine (a) the relative standard deviations of the calibration measurements (day 1 and day 2/3 were measured with different batches of fluorescamine) and (b) the particle surface characterization. The mean results obtained for (1) NanoChOp-01, (2) SiO_2-NH_2@UCNP, and (4) SiO_2 NP-NH_2 revealed lower amounts of amino FGs compared to the estimated maximum values for the reporter coverage of the particle surface, while for (2) SiO_2-NH_2@IONP, higher amounts were obtained. (c) Emission spectra of fluorescamine (black line; (λ_{ex} = 392 nm)) and the aminated particles, shown exemplary for NanoChOp-01, SiO_2 NP-NH_2, and SiO_2-NH_2@IONP as well as for EA after incubation with fluorescamine. (d) Emission spectra of the non-aminated NPs and l-valine used as positive controls recorded after incubation with fluorescamine.

the importance of proper pipette adjustment and pipetting technique [42–44]. Also, the collected additional information on the operator provided first hints on the influence of the operator skills and training on the accuracy and reliability of the assay results.

As revealed by the study outcome, assay precision and accuracy considerably varied amongst the participants due to the different performance in the sample preparation and sample transfer steps. Other sources of uncertainty included the unintentional exchange of samples or the lack of reactant addition as shown for the calibration curves in Figs. S13 and S14, and Table S1 in the ESM. A direct measure for the comparison of the accuracy and reliability of the automated and manually performed Fluram assay provides the coefficient of determination (COD) of the calibration curves. While the usage of the pipetting robot yielded COD values of 0.9938 and 0.9925 for set1 and set2, for the manual Fluram assays the COD values varied between 0.1994–0.9979 depending on the experience of the participants (Fig. 4(a)). The results of the positive control with a known concentration of L-valine revealed values in the range of the uncertainty of the pipettes for the robot and participants 10 and 11, while all other participants overestimated the amount of fluorescamine in the sample (Fig. 4(b)). The positive control was also used to assess the accuracy of the results. The automated performance of the Fluram assay with the pipetting robot resulted in small coefficients of variation for all tested particles and yielded values below the estimated maximum probe coverage (Figs. 4(c), 4(d), and 4(f)), that was comparable to the result obtained from the experienced scientist (Fig. S15 in the ESM). Only the results obtained for the SiO_2-NH_2@IONP were higher (Fig. 4(e)). The results of the manually performed assays varied widely (Figs. 4(c)–4(f)).

As standardized optical assays should have defined time limits for each pipetting step to ensure data consistency, the time dedicated to the generation of the calibration curve and the filling of the 96-well microtiter plates (Fig. S16 in the ESM) were recorded by each participant. The calculated total time included the pipetting steps and the time required for assay incubation. This time frame varied between 64 to 125 min amongst participants. Workflow automation with the pipetting robot ensured that each microtiter plate was prepared utilizing the same amount of time, here 69 and 72 min. This led to a considerably improved plate-to-plate and day-to-day data consistency. Thereby, also possible influences of reagent instabilities could be easily considered and circumvented. With simple automation, the hands-on preparation time of the Fluram assay could be significantly reduced from an average of 79:23 min to 10 to 15 min. For a working day of 8 h, 6 assays can be run per day and with a complete automation approach, the assays can be principally performed 24/7.

4 Conclusion and outlook

The meanwhile recognized importance of screening, monitoring, and quantifying surface FGs on nanoparticles for process, stability, and quality control as well as for an improved NP performance and risk assessment requires fast, broadly available, and cost-efficient methods and validated workflows for the characterization of NP surface chemistry. Here, optical assays can provide ideal tools which can be automated, thereby exploiting the expertise

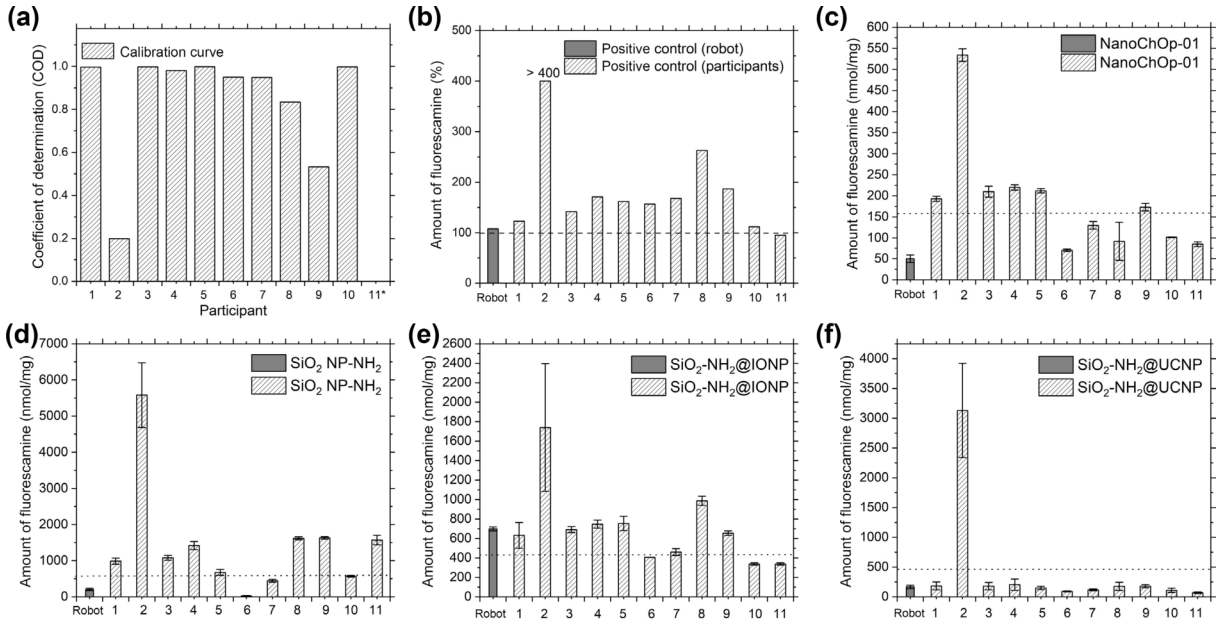

Figure 4 Overview of the results obtained from the manually performed and the automated Fluram assay involving manual pipetting by 11 operators and a pipetting robot. (a) Comparison of the obtained COD of the assay calibration (*no calibration curve was obtained); Comparison of the results obtained for (b) the positive control (dashed line = 100%; dark grey = results of the robot), (c) NanoChOp-01 (dashed line = maximum estimated probe coverage (158.80 nmol/mg)), (d) SiO_2 NP-NH_2 (dashed line = maximum estimated probe coverage (566.11 nmol/mg)), (e) SiO_2-NH_2@IONP (dashed line = maximum estimated probe coverage (432.66 nmol/mg)), and (f) SiO_2-NH_2@UCNP (dashed line = maximum estimated probe coverage (458.55 nmol/mg)). All results of the aminated NPs (c)–(f) shown for the measurements with the robot relate to set 1.

from already largely automated areas such as clinical diagnostics and drug development. Although such assay can commonly not quantify the exact coverage of FGs or their total number, they present very valuable tools for quality and process control, the determination of batch-to-batch reproducibilities, and the monitoring of particle stability and aging.

To highlight the potential of simple automation tools such as pipetting robots in combination with optical assays for surface FG analysis on nanomaterials, we exemplarily explored the quantification of amino surface FGs on different types of broadly utilized NPs, varying in size, chemical composition, and optical properties, with the Fluram assay relying on the chromogenic reporter fluorescamine. The comparison of the assay results obtained by automated and manual pipetting steps and automated assay readout underlined the advantages of automated workflows for data accuracy, data consistency, and speed of analysis also for surface group quantification. Given the provided insights into the expertise, experimental skills, and training of the 11 study participants, also typical human-related sources of uncertainty in pipetting steps and assay performance could be revealed that can be elegantly circumvented by automation. This, however, requires proper validation of the instrumentation including hardware, e.g., pipettes for pipetting robots, and software.

This first-time simple and cost-efficient automation of an optical assay for quantifying surface FGs on broadly utilized NPs and its comparison with the results of manual assay performance highlights the huge automation potential in the area of nanotechnology. This can be further advanced by exploiting different automation tools developed for other fields of application and can pave the road to produce large data sets for assessing sustainable and safer by design approaches and particularly for nanomaterial grouping for nanomaterial risk assessment and functionality studies. In the future, we will assess the applicability of the automated assay workflow for different types of nanomaterials, thereby also deriving requirements on negative and positive controls, and expand this concept to other FGs and optical reporters. Also, other methods for surface characterization such as zeta potential measurements and pH titrations should be easily accessible to automation.

Author contribution statement

I. T. developed the assay protocol, organized, and analyzed the pipetting study. I. T. and U. R. designed the study and wrote the first drafts of the manuscript. I. T. and A. M. synthesized and characterized the surface-functionalized nanoparticles, and I. T. and K. S. R. developed the methods of the optical assays for the pipetting robot. C. M. performed the titration experiments to determine the total number of the functional groups. All authors contributed to the final version of the manuscript.

Acknowledgements

The authors would like to thank the members of Division Biophotonics (BAM-1.2) to participate and to support the pipetting contest. Parts of this work were performed at the electron microscopy center at BAM. The authors acknowledge Carsten Prinz from Division Structure Analysis for preparation of the TEM images and Dr. Elina Andresen from Division Biophotonics for synthesis of the upconversion nanoparticle cores.

Electronic Supplementary Material: Supplementary material (further details of the amination step of the synthesized nanoparticles, the quantification of the total and derivatizable number of amino FGs, TEM micrographs, DLS results, optical properties measurements, and results of the questionnaire) is available in the online version of this article at https://doi.org/10.1007/s12274-024-6970-1.

References

[1] Dai, W. G.; Pollock-Dove, C.; Dong, L. C.; Li, S. Advanced screening assays to rapidly identify solubility-enhancing formulations: High-throughput, miniaturization and automation. *Adv. Drug Deliv. Rev.* **2008**, *60*, 657–672.

[2] Ahene, A. B.; Morrow, C.; Rusnak, D.; Spitz, S.; Usansky, J.; Pils, H.; Civoli, F.; Pandya, K.; Sue, B.; Leach, D. et al. Ligand binding assays in the 21st century laboratory: Automation. *AAPS J.* **2012**, *14*, 142–153.

[3] Ray, C. A.; Ahene, A. B. Ligand binding assays in the 21st century laboratory-a call for change. *AAPS J.* **2012**, *14*, 377–379.

[4] Fang, X. N.; Zheng, Y. Z.; Duan, Y. K.; Liu, Y.; Zhong, W. W. Recent advances in design of fluorescence-based assays for high-throughput screening. *Anal. Chem.* **2019**, *91*, 482–504.

[5] Hecko, S.; Schiefer, A.; Badenhorst, C. P. S.; Fink, M. J.; Mihovilovic, M. D.; Bornscheuer, U. T.; Rudroff, F. Enlightening the path to protein engineering: Chemoselective turn-on probes for high-throughput screening of enzymatic activity. *Chem. Rev.* **2023**, *123*, 2832–2901.

[6] Hess, J. F.; Kohl, T. A.; Kotrová, M.; Rönsch, K.; Paprotka, T.; Mohr, V.; Hutzenlaub, T.; Brüggemann, M.; Zengerle, R.; Niemann, S. et al. Library preparation for next generation sequencing: A review of automation strategies. *Biotechnol. Adv.* **2020**, *41*, 107537.

[7] Holland, I.; Davies, J. A. Automation in the life science research laboratory. *Front. Bioeng. Biotechnol.* **2020**, *8*, 571777.

[8] Christensen, M.; Yunker, L. P. E.; Shiri, P.; Zepel, T.; Prieto, P. L.; Grunert, S.; Bork, F.; Hein, J. E. Automation isn't automatic. *Chem. Sci.* **2021**, *12*, 15473–15490.

[9] Abolhasani, M.; Kumacheva, E. The rise of self-driving labs in chemical and materials sciences. *Nat. Synth.* **2023**, *2*, 483–492.

[10] Taguchi, S.; Suda, Y.; Irie, K.; Ozaki, H. Automation of yeast spot assays using an affordable liquid handling robot. *SLAS Technol.* **2023**, *28*, 55–62.

[11] Manzano, J. S.; Hou, W. D.; Zalesskiy, S. S.; Frei, P.; Wang, H.; Kitson, P. J.; Cronin, L. An autonomous portable platform for universal chemical synthesis. *Nat. Chem.* **2022**, *14*, 1311–1318.

[12] Li, Y. C.; Xia, L. L.; Fan, Y. M.; Wang, Q. Y.; Hu, M. Recent advances in autonomous synthesis of materials. *ChemPhysMater* **2022**, *1*, 77–85.

[13] Dembski, S.; Schwarz, T.; Oppmann, M.; Bandesha, S. T.; Schmid, J.; Wenderoth, S.; Mandel, K.; Hansmann, J. Establishing and testing a robot-based platform to enable the automated production of nanoparticles in a flexible and modular way. *Sci. Rep.* **2023**, *13*, 11440.

[14] Xing, C. Y.; Chen, G. Y.; Zhu, X.; An, J. K.; Bao, J. C.; Wang, X.; Zhou, X. Q.; Du, X. L.; Xu, X. X. Synthesis of carbon dots with predictable photoluminescence by the aid of machine learning. *Nano Res.* **2024**, *17*, 1984–1989.

[15] Rietscher, R.; Thum, C.; Lehr, C. M.; Schneider, M. Semi-automated nanoprecipitation-system-an option for operator independent, scalable and size adjustable nanoparticle synthesis. *Pharm. Res.* **2015**, *32*, 1859–1863.

[16] Epps, R. W.; Bowen, M. S.; Volk, A. A.; Abdel-Latif, K.; Han, S. Y.; Reyes, K. G.; Amassian, A.; Abolhasani, M. Artificial chemist: An autonomous quantum dot synthesis bot. *Adv. Mater.* **2020**, *32*, 2001626.

[17] Salley, D.; Keenan, G.; Grizou, J.; Sharma, A.; Martín, S.; Cronin, L. A nanomaterials discovery robot for the Darwinian evolution of shape programmable gold nanoparticles. *Nat. Commun.* **2020**, *11*, 2771.

[18] Chan, E. M. Combinatorial approaches for developing upconverting nanomaterials: High-throughput screening, modeling, and applications. *Chem. Soc. Rev.* **2015**, *44*, 1653–1679.

[19] Lüdicke, M. G.; Hildebrandt, J.; Schindler, C.; Sperling, R. A.; Maskos, M. Automated quantum dots purification via solid phase extraction. *Nanomaterials* **2022**, *12*, 1983.

[20] Xia, X. J.; Sivonxay, E.; Helms, B. A.; Blau, S. M.; Chan, E. M. Accelerating the design of multishell upconverting nanoparticles through Bayesian optimization. *Nano Lett.* **2023**, *23*, 11129–11136.

[21] Salaheldin, A. M.; Walter, J.; Herre, P.; Levchuk, I.; Jabbari, Y.; Kolle, J. M.; Brabec, C. J.; Peukert, W.; Segets, D. Automated synthesis of quantum dot nanocrystals by hot injection: Mixing induced self-focusing. *Chem. Eng. J.* **2017**, *320*, 232–243.

[22] Jiang, Y. B.; Salley, D.; Sharma, A.; Keenan, G.; Mullin, M.; Cronin, L. An artificial intelligence enabled chemical synthesis robot for exploration and optimization of nanomaterials. *Sci. Adv.* **2022**, *8*, eabo2626.

[23] Murthy, C. R.; Gao, B.; Tao, A. R.; Arya, G. Automated quantitative image analysis of nanoparticle assembly. *Nanoscale* **2015**, *7*, 9793–9805.

[24] Wang, X.; Zeng, Q.; Xie, F.; Wang, J. A.; Yang, Y. T.; Xu, Y.; Li, J. H.; Yu, H. Automated nanoparticle analysis in surface plasmon resonance microscopy. *Anal. Chem.* **2021**, *93*, 7399–7404.

[25] Geißler, D.; Wegmann, M.; Jochum, T.; Somma, V.; Sowa, M.; Scholz, J.; Fröhlich, E.; Hoffmann, K.; Niehaus, J.; Roggenbuck, D. et al. An automatable platform for genotoxicity testing of nanomaterials based on the fluorometric γ-H2AX assay reveals no genotoxicity of properly surface-shielded cadmium-based quantum dots. *Nanoscale* **2019**, *11*, 13458–13468.

[26] Egbuna, C.; Parmar, V. K.; Jeevanandam, J.; Ezzat, S. M.; Patrick-Iwuanyanwu, K. C.; Adetunji, C. O.; Khan, J.; Onyeike, E. N.; Uche, C. Z.; Akram, M. et al. Toxicity of nanoparticles in biomedical application: Nanotoxicology. *J. Toxicol.* **2021**, *2021*, 9954443.

[27] Kim, S. T.; Saha, K.; Kim, C.; Rotello, V. M. The role of surface functionality in determining nanoparticle cytotoxicity. *Acc. Chem. Res.* **2013**, *46*, 681–691.

[28] Jeliazkova, N.; Bleeker, E.; Cross, R.; Haase, A.; Janer, G.; Peijnenburg, W.; Pink, M.; Rauscher, H.; Svendsen, C.; Tsiliki, G. et al. How can we justify grouping of nanoforms for hazard assessment? Concepts and tools to quantify similarity. *NanoImpact* **2022**, *25*, 100366.

[29] Kunc, F.; Nirmalananthan-Budau, N.; Rühle, B.; Sun, Y.; Johnston, L. J.; Resch-Genger, U. Interlaboratory comparison on the quantification of total and accessible amine groups on silica nanoparticles with qNMR and optical assays. *Anal. Chem.* **2021**, *93*, 15271–15278.

[30] Geißler, D.; Nirmalananthan-Budau, N.; Scholtz, L.; Tavernaro, I.; Resch-Genger, U. Analyzing the surface of functional nanomaterials-how to quantify the total and derivatizable number of functional groups and ligands. *Microchim. Acta* **2021**, *188*, 321.

[31] Luo, H.; Tian, L.; Zhang, Y.; Wu, Y.; Li, B.; Liu, J. *Nano Res*. **2024**.

[32] Quevedo, P. D.; Behnke, T.; Resch-Genger, U. Streptavidin conjugation and quantification-a method evaluation for nanoparticles. *Anal. Bioanal. Chem.* **2016**, *408*, 4133–4149.

[33] Chatterjee, K.; Sarkar, S.; Jagajjanani Rao, K.; Paria, S. Core/shell nanoparticles in biomedical applications. *Adv. Colloid Interface Sci.* **2014**, *209*, 8–39.

[34] Pallavi, P.; Harini, K.; Alshehri, S.; Ghoneim, M. M.; Alshlowi, A.; Gowtham, P.; Girigoswami, K.; Shakeel, F.; Girigoswami, A. From synthetic route of silica nanoparticles to theranostic applications. *Processes* **2022**, *10*, 2595.

[35] Spoială, A.; Ilie, C. I.; Crăciun, L. N.; Ficai, D.; Ficai, A.; Andronescu, E. Magnetite-silica core/shell nanostructures: From surface functionalization towards biomedical applications-a review. *Appl. Sci.* **2021**, *11*, 11075.

[36] Borse, S.; Rafique, R.; Murthy, Z. V. P.; Park, T. J.; Kailasa, S. K. Applications of upconversion nanoparticles in analytical and biomedical sciences: A review. *Analyst* **2022**, *147*, 3155–3179.

[37] Felbeck, T.; Hoffmann, K.; Lezhnina, M. M.; Kynast, U. H.; Resch-Genger, U. Fluorescent nanoclays: Covalent functionalization with amine reactive dyes from different fluorophore classes and surface group quantification. *J. Phys. Chem. C* **2015**, *119*, 12978–12987.

[38] Moser, M.; Nirmalananthan, N.; Behnke, T.; Geißler, D.; Resch-Genger, U. Multimodal cleavable reporters versus conventional labels for optical quantification of accessible amino and carboxy groups on nano- and microparticles. *Anal. Chem.* **2018**, *90*, 5887–5895.

[39] Chen, Y.; Zhang, Y. Q. Fluorescent quantification of amino groups on silica nanoparticle surfaces. *Anal. Bioanal. Chem.* **2011**, *399*, 2503–2509.

[40] Hsiao, I. L.; Fritsch-Decker, S.; Leidner, A.; Al-Rawi, M.; Hug, V.; Diabaté, S.; Grage, S. L.; Meffert, M.; Stoeger, T.; Gerthsen, D. et al. Biocompatibility of amine-functionalized silica nanoparticles: The role of surface coverage. *Small* **2019**, *15*, 1805400.

[41] Derayea, S. M.; Samir, E. A review on the use of fluorescamine as versatile and convenient analytical probe. *Microchem. J.* **2020**, *156*, 104835.

[42] Guan, X. L.; Chang, D. P. S.; Mok, Z. X.; Lee, B. Assessing variations in manual pipetting: An under-investigated requirement of good laboratory practice. *J. Mass Spectrom. Adv. Clin. Lab* **2023**, *30*, 25–29.

[43] Pandya, K.; Ray, C. A.; Brunner, L.; Wang, J.; Lee, J. W.; DeSilva, B. Strategies to minimize variability and bias associated with manual pipetting in ligand binding assays to assure data quality of protein therapeutic quantification. *J. Pharm. Biomed. Anal.* **2010**, *53*, 623–630.

[44] Lippi, G.; Lima-Oliveira, G.; Brocco, G.; Bassi, A.; Salvagno, G. L. Estimating the intra- and inter-individual imprecision of manual pipetting. *Clin. Chem. Lab. Med.* **2017**, *55*, 962–966.

[45] Schmidt, S.; Tavernaro, I.; Cavelius, C.; Weber, E.; Kümper, A.; Schmitz, C.; Fleddermann, J.; Kraegeloh, A. Silica nanoparticles for intracellular protein delivery: A novel synthesis approach using green fluorescent protein. *Nanoscale Res. Lett.* **2017**, *12*, 545.

[46] Ding, H. L.; Zhang, Y. X.; Wang, S.; Xu, J. M.; Xu, S. C.; Li, G. H. Fe_3O_4@SiO_2 core/shell nanoparticles: The silica coating regulations with a single core for different core sizes and shell thicknesses. *Chem. Mater.* **2012**, *24*, 4572–4580.

[47] Roebben, G.; Kestens, V.; Varga, Z.; Charoud-Got, J.; Ramaye, Y.; Gollwitzer, C.; Bartczak, D.; Geißler, D.; Noble, J.; Mazoua, S. et al. Reference materials and representative test materials to develop nanoparticle characterization methods: The NanoChOp project case. *Front. Chem.* **2015**, *3*, 56.

[48] Dietrich, P. M.; Streeck, C.; Glamsch, S.; Ehlert, C.; Lippitz, A.; Nutsch, A.; Kulak, N.; Beckhoff, B.; Unger, W. E. S. Quantification of silane molecules on oxidized silicon: Are there options for a traceable and absolute determination. *Anal. Chem.* **2015**, *87*, 10117–10124.

[49] Sun, Y.; Kunc, F.; Balhara, V.; Coleman, B.; Kodra, O.; Raza, M.; Chen, M. H.; Brinkmann, A.; Lopinski, G. P.; Johnston, L. J. Quantification of amine functional groups on silica nanoparticles: A multi-method approach. *Nanoscale Adv.* **2019**, *1*, 1598–1607.

[50] Ashby, J.; Duan, Y. K.; Ligans, E.; Tamsi, M.; Zhong, W. W. High-throughput profiling of nanoparticle-protein interactions by fluorescamine labeling. *Anal. Chem.* **2015**, *87*, 2213–2219.

[51] Murugayah, S. A.; Warring, S. L.; Gerth, M. L. Optimisation of a high-throughput fluorescamine assay for detection of N-acyl-L-homoserine lactone acylase activity. *Anal. Biochem.* **2019**, *566*, 10–12.

[52] Li, Z.; Xue, Z. W.; Wu, Z. S.; Han, J. H.; Han, S. F. Chromo-fluorogenic detection of aldehydes with a rhodamine based sensor featuring an intramolecular deoxylactam. *Org. Biomol. Chem.* **2011**, *9*, 7652–7654.

[53] Ros-Lis, J. V.; Martínez-Máñez, R.; Soto, J. A selective chromogenic reagent for cyanide determination. *Chem. Commun.* **2002**, 2248–2249

[54] Li, X. H.; Gao, X. H.; Shi, W.; Ma, H. M. Design strategies for water-soluble small molecular chromogenic and fluorogenic probes. *Chem. Rev.* **2014**, *114*, 590–659.

[55] Hennig, A.; Borcherding, H.; Jaeger, C.; Hatami, S.; Würth, C.; Hoffmann, A.; Hoffmann, K.; Thiele, T.; Schedler, U.; Resch-Genger, U. Scope and limitations of surface functional group quantification methods: Exploratory study with poly(acrylic acid)-grafted micro- and nanoparticles. *J. Am. Chem. Soc.* **2012**, *134*, 8268–8276.